

## Vibrational spectrum of solid picene ( $C_{22}H_{14}$ )

B. Joseph,<sup>1</sup> L. Boeri,<sup>2</sup> L. Malavasi,<sup>3</sup> F. Capitani,<sup>1</sup> G.A. Artioli,<sup>3</sup> S. Protti,<sup>3</sup> M. Fagnoni,<sup>3</sup> A. Albini,<sup>3</sup> C. Marini,<sup>4</sup> L. Baldassarre\*,<sup>5</sup> A. Perucchi,<sup>5</sup> S. Lupi,<sup>6</sup> P. Postorino,<sup>6</sup> and P. Dore<sup>7, †</sup>

<sup>1</sup>*Dipartimento di Fisica, Università di Roma Sapienza, P.le Aldo Moro 2, 00185 Roma, Italy*

<sup>2</sup>*Max Planck Institute for Solid State Research, Heisenbergstrasse 1, D-70569, Stuttgart, Germany*

<sup>3</sup>*Dipartimento di Chimica, Università di Pavia, Via Taramelli, 27100 Pavia, Italy*

<sup>4</sup>*European Synchrotron Radiation Facility, BP 220, 38043 Grenoble Cedex, France*

<sup>5</sup>*Sincrotrone Trieste, S.C.p.A., Area Science Park, I-34012, Basovizza, Trieste, Italy*

<sup>6</sup>*CNR-IOM and Dipartimento di Fisica, Università di Roma Sapienza, P.le Aldo Moro 2, 00185 Roma, Italy*

<sup>7</sup>*CNR-SPIN and Dipartimento di Fisica, Università di Roma Sapienza, P.le Aldo Moro 2, 00185 Roma, Italy*

Recently, Mitsuhashi *et al* have observed superconductivity with transition temperature up to 18 K in potassium doped picene ( $C_{22}H_{14}$ ), a polycyclic aromatic hydrocarbon compound [*Nature* **464** (2010) 76]. Theoretical analysis indicate the importance of electron-phonon coupling in the superconducting mechanisms of these systems, with different emphasis on inter- and intra-molecular vibrations, depending on the approximations used. Here we present a combined experimental and ab-initio study of the Raman and infrared spectrum of undoped solid picene, which allows us to unambiguously assign the vibrational modes. This combined study enables the identification of the modes which couple strongly to electrons and hence can play an important role in the superconducting properties of the doped samples.

Journal reference : *Journal of Physics: Condensed Matter* **24** (2012) 252203

PACS numbers: 74.25.Kc, 74.70.Kn, 74.25.Gz, 71.15.Mb

---

\* Present address: Center for Life NanoScience@LaSapienza, Istituto Italiano di Tecnologia, Viale Regina Elena 295, Roma, Italy

Recently, superconductivity has been observed in potassium doped picene, with transition temperatures  $T_c$  of 7-18 K<sup>1</sup>. This was the first report on "high- $T_c$ " superconductivity (SC) in an aromatic compound. Picene ( $C_{22}H_{14}$ ) is an alternant polycyclic aromatic hydrocarbon (PAH), *i.e.* a planar aromatic molecule, formed by juxtaposed benzene rings. Picene comprises five rings, arranged in a zig-zag fashion. After this initial report, SC was also reported in phenanthrene (three rings)<sup>2</sup>, dibenzpentalene (five + two rings)<sup>3</sup> and coronene (six rings)<sup>4</sup> upon doping with alkali or alkali-earth metals. SC was then also observed in picene and phenanthrene doped with rare-earths<sup>4-6</sup>, indicating that the PAHs most likely form a completely new class of superconductors, with highly *tunable* electronic properties.

Due to their 2-dimensional nature, PAHs are naturally related to other *layered* superconductors, such as  $MgB_2$ <sup>7</sup>, or the newly-proposed graphane<sup>8</sup>. However, in contrast to all these systems, which are conventional electron-phonon (*ep*) superconductors, the nature and origin of SC in PAH are still debated. Theoretical studies have focused either on electron-electron (*ee*)<sup>9,10</sup> or *ep* interaction<sup>11-14</sup>, which are both sizable in these  $\pi$ -bonded systems. However, estimates of strength and spectral distribution of the *ep* interaction differ depending on the approximation used for doping. The main question is to establish how much the *ep* coupling in an isolated molecule picture is representative of coupling in the actual doped compound<sup>11-13</sup>. A definite answer on this point could only come from a detailed experimental comparison of the phonon spectra and lifetimes of the doped and undoped samples. This has not been possible so far, because the vibrational spectra are extremely rich, and the samples are poorly characterized. For the doped superconducting samples in ref.<sup>1</sup>, not only the detailed crystal structure, but also the precise doping level are unknown. For pure picene, X-ray diffraction profiles have been refined several years ago<sup>15</sup>, but, owing to the lack of high-purity samples, there were no serious attempts to a complete characterization of the vibrational spectrum, except for a recent study of the optical phonons<sup>16</sup>, which appeared in the literature while we were finalizing the present manuscript.

In this paper, we present a combined experimental and theoretical study<sup>17,18</sup> of the vibrational spectrum of crystalline picene, based on accurate Raman and infrared measurements at room temperature on high quality samples. Density functional perturbation theory (DFPT<sup>19</sup>) calculations were also performed, which allowed us to obtain a detailed assignment of vibrational modes. This study is propaedeutical to further studies on the high-pressure behaviour of doped and undoped samples, which could lead to significant insights into the importance of intermolecular coupling of vibrational modes and electrons in hydrocarbons, and on the reliability of DFT in organic compounds<sup>20</sup>. Besides superconductivity, our study is of interest also for potential applications in organic electronics<sup>4,21</sup>.

Solid picene was prepared by a new optimized synthesis route which permits to obtain bulk quantities (hundreds of milligrams in one shot) of pure polycrystalline picene powder<sup>22</sup>. Refinements of the X-ray diffraction spectrum of our sample yielded results identical to those previously reported<sup>15</sup>. We performed Raman measurements by means of a confocal-microscope Raman spectrometer, equipped with a He-Ne laser ( $\lambda=632.8$  nm), a 1800 lines-mm<sup>-1</sup> grating monochromator, and a charge-coupled-device (CCD) detector. Raman measurements were carried out on the powder samples in the backscattering geometry, and a notch filter was used to reject the elastic contribution. Using a few micron-sized laser spot on the sample, accurate Raman spectra were collected with a spectral resolution better than 3 cm<sup>-1</sup>. A typical Raman spectrum is reported in Fig. 1(a) over the frequency range 200-1700 cm<sup>-1</sup>. Note that intensity and width of the highest and sharpest peaks may be affected by the instrumental spectral resolution. For infrared (IR) measurements, we employed a thin pellet (of thickness around 50 micron) prepared out of pure picene powder. IR transmittance measurements were carried out at the SISSI infrared beamline of the ELETTRA synchrotron

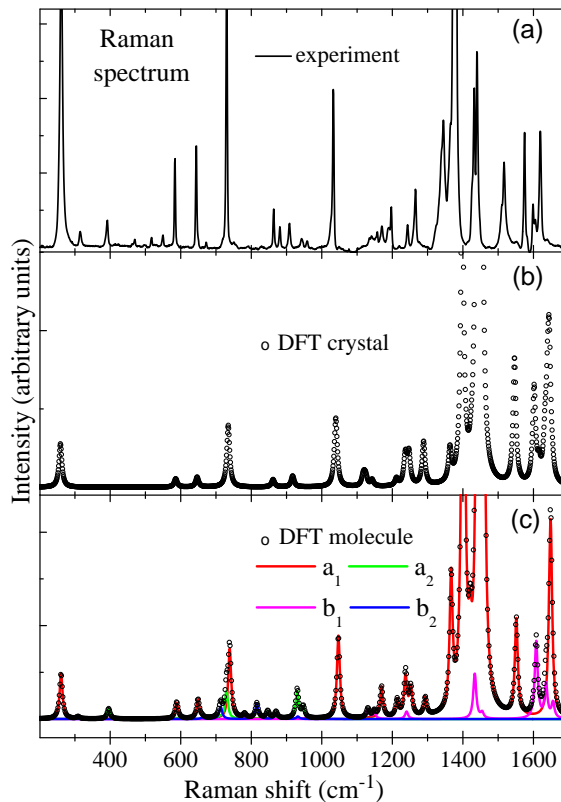


FIG. 1: (Color online) Comparison of the experimental Raman spectrum of crystalline picene (a) with the DFT spectrum of crystal (b) and relaxed molecule (c). For the molecule, the spectral components of different symmetry ( $a_1$ ,  $b_1$ ,  $a_2$ ,  $b_2$ ) are shown separately (see text for details). The computed DFT stick spectra are convoluted with a Lorentzian profile with  $5 \text{ cm}^{-1}$  linewidth to ease comparison with experiment.

(Trieste, Italy)<sup>23</sup>. Using a Bruker IFS 66v interferometer equipped with both mylar beam splitters coupled to a liquid He bolometer for the far-IR region and a KBr beam splitter coupled to a mercury-cadmium-telluride (MCT) detector for the mid-IR region, accurate IR spectra with a spectral resolution close to  $2 \text{ cm}^{-1}$  were collected. A typical IR spectrum is reported in Fig. 2(a) over the frequency range  $200\text{-}1700 \text{ cm}^{-1}$ . We notice that the most intense absorption lines result from vanishingly small transmitted intensities. These lines can therefore be affected by rather large uncertainties. Nevertheless, a large number of low intensity absorption peaks are determined with a good accuracy.

The Raman and IR spectra of picene in its crystalline and molecular forms have been calculated using DFT<sup>19,24,25</sup>. The electron-ion interaction was described using LDA norm-conserving pseudopotentials<sup>26</sup>; electronic wavefunctions were expanded on a plane-wave basis, with a 80 Ryd cutoff. A  $2^3$  uniform grid for  $\mathbf{k}$ -space integration in the solid allowed an accuracy of  $\pm 5 \text{ cm}^{-1}$  on the calculated frequencies. For the crystal, we employed the experimental unit cell, and relaxed atomic positions. The resulting Raman and IR spectra are reported in Figs. 1(b) and 2(b), respectively. For the molecule, we employed periodical repetitions of a  $24 \times 10 \times 5 \text{ \AA}$  supercell, containing a single picene molecule, with the  $z$  axis orthogonal to the  $ab$  plane, and the long molecular axis along the  $x$  axis. The cut-off energy was rescaled accordingly. We performed calculations both for an ideal geometry, and for a relaxed geometry in which we optimized the internal coordinates subject to the constraint of symmetry. The resulting Raman and IR

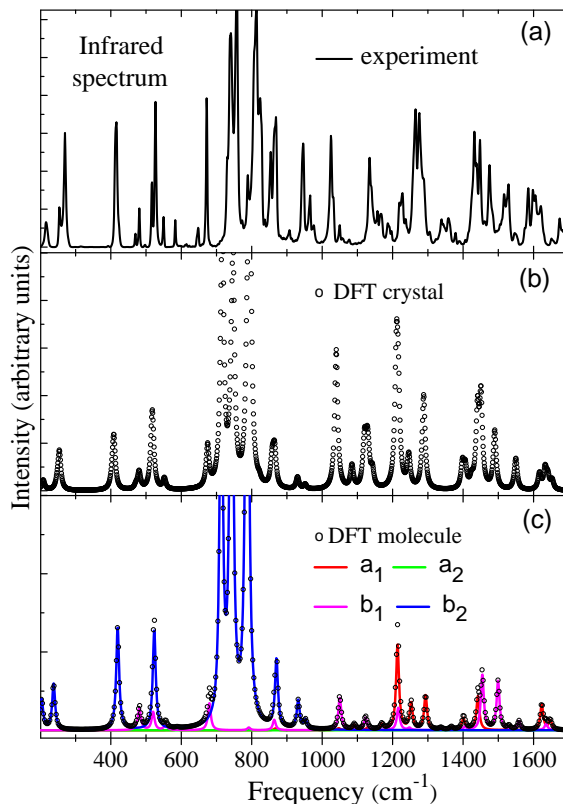


FIG. 2: (Color online) Same as Fig. 1, for the IR spectra.

spectra are reported in Figs. 1(c) and 2(c), respectively. Note that the results we report in these figures are for the relaxed molecular geometry, but the difference between the ideal and relaxed molecule spectra is never larger than  $\pm 10 \text{ cm}^{-1}$ .

In comparing the measured and the calculated spectra, it is convenient to recall that the calculated partial phonon density of states (not shown) indicates that modes up to  $1000 \text{ cm}^{-1}$  involve both out-of-plane and in-plane vibrations of carbon and hydrogen; above  $1000 \text{ cm}^{-1}$ , the vibrations are only in-plane, with high-energy vibrations above  $3000 \text{ cm}^{-1}$  involving only H atoms.<sup>12</sup> The unit cell of crystalline picene is monoclinic (space group  $P2_1$ ) and contains two  $\text{C}_{22}\text{H}_{14}$  molecules, arranged in a herringbone fashion and inclining slightly to the  $ab$  plane. This yields 216 vibrational modes, many of which are both IR and Raman active. The comparison of the upper and middle panels of the two figures gives an idea of the accuracy of DFT calculations: DFT captures many of the main features of the experimental spectra, including the positions, intensities and splitting of the main peaks, with a few exceptions. The lower panel of the two figures shows the equivalent spectra, calculated for the picene molecule; the symbols show the total intensities, while colored lines refer to the four possible symmetries for the vibrational modes. The picene molecule has  $C_{2v}$  symmetry; of the 102 optical modes, those with  $a_1$  (35),  $b_2$  (16),  $b_1$  (34) symmetry are both Raman and IR active, while the  $a_2$  (17) are only Raman-active<sup>27</sup>. A full list of peak frequency, symmetry, optical activity and the normalized intensity of the vibrational modes is given in the supplementary information file. It is worth noting that, for an isolated molecule, the Raman response is dominated by the (totally symmetric)  $a_1$  modes (Fig. 1(c)), the IR response by the  $b_2$  modes (Fig. 2(c)).

From a comparison between the calculated crystal and molecule spectra (see Figs. 1 and 2), it can be observed that

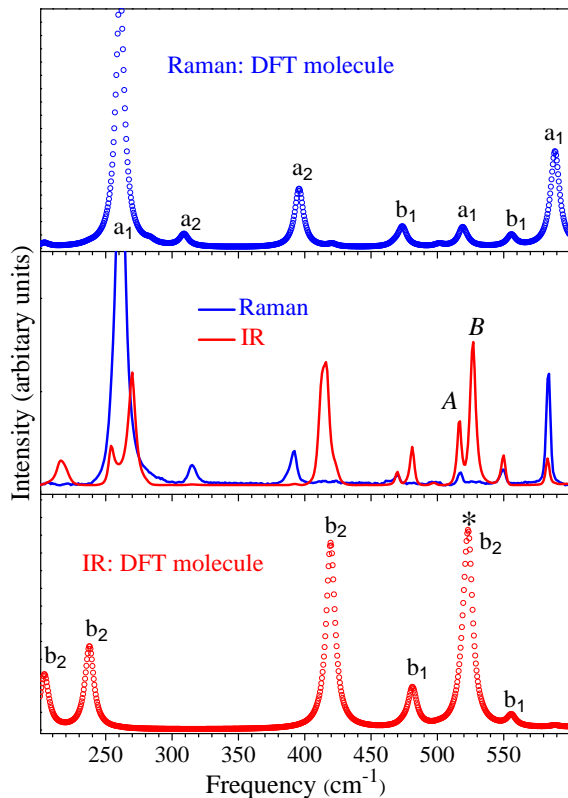


FIG. 3: (Color online) Comparison between the measured IR and Raman spectra (middle panel) and DFT Raman (upper panel) and IR (lower panel) spectra in the range 200 - 600  $\text{cm}^{-1}$ . The computed DFT stick spectra are convoluted with a Lorentzian profile with 10  $\text{cm}^{-1}$  linewidth to ease comparison with experiment. Similar comparisons at higher frequencies are given in the supplementary information file. In the IR DFT spectrum of the molecule (lower panel), the  $b_2$  peak at 523  $\text{cm}^{-1}$  marked by \* splits into  $A$  and  $B$  components (see text) in the measured spectrum (middle panel).

the molecular modes dominate the optical response. Picene is thus a typical molecular crystal, in which the optical response is determined by the selection rules due to the point group of the molecule, on which the site group of the crystal acts as a perturbation<sup>28</sup>.

Given the overall agreement between the spectra calculated for the molecule and the crystal, we have used the molecular symmetry assignments to label the vibrational modes observed in the solid. Fig. 3 shows a detailed comparison between the experimental (Raman and IR) and the calculated (molecule) spectra in the energy range between 200 and 600  $\text{cm}^{-1}$ . Similar comparisons at higher frequencies are given in the supplementary information file. In the same file we also report results obtained in the frequency range of the C-H stretching (3000-3250  $\text{cm}^{-1}$ ), which is not of direct interest in the present work. Exploiting this kind of plots and of comparisons, we have been able to make a reliable assignments of most of the observed vibrational peaks.

In Table 1, we provide the list of the most intense peaks which can be assigned without ambiguity. Our results extend a recent study<sup>16</sup>, which contains a partial assignment of the vibrational modes of picene, based on optical measurements and calculations<sup>29</sup>. Note that in correspondence to some of the DFT lines computed for the molecule, a doublet is observed; this effect can be attributed to the Davydov splitting of two modes corresponding to the same molecular vibration<sup>16</sup>. For example, in Fig. 3 (see lower panel) the  $b_2$  peak at 523  $\text{cm}^{-1}$  marked by \* splits into two

TABLE I: Assignment of the most intense vibrational modes observed. For each mode, the frequency, symmetry and optical activity calculated in DFT are reported together with the corresponding IR and/or Raman frequency. All frequencies are in  $\text{cm}^{-1}$ . The  $a_1$  modes expected to be most involved in the *ep* coupling<sup>13</sup> are marked by \*. A complete list of frequencies and intensities of all the modes calculated in DFT is provided in the supplementary information file.

Frequency DFT	Mode	Activity	Frequency IR	Frequency Raman
203.8	b <sub>2</sub>	I+R	217	
237.8	b <sub>2</sub>	I+R	254 , 270	
260.8	a <sub>1</sub>	I+R		262*
309.0	a <sub>2</sub>	R	–	314
395.8	a <sub>2</sub>	R	–	391
419.5	b <sub>2</sub>	I+R	415	
481.2	b <sub>1</sub>	I+R	481	
523.3	b <sub>2</sub>	I+R	517 , 527	517
555.8	b <sub>1</sub>	I+R	550	550
588.5	a <sub>1</sub>	I+R	584	584
649.2	a <sub>1</sub>	I+R		644
679.8	b <sub>1</sub>	I+R	672	
713.4	b <sub>2</sub>	I+R	740 , 756	
738.9	a <sub>1</sub>	I+R		730*
742.5	b <sub>2</sub>	I+R	810	
787.0	b <sub>2</sub>	I+R	853 , 865	
867.3	a <sub>1</sub>	I+R		864
870.2	b <sub>2</sub>	I+R		
930.2	a <sub>2</sub>	R	–	908
932.1	b <sub>2</sub>	I+R	947	
1047.1	a <sub>1</sub>	I+R		1032
1050.1	b <sub>1</sub>	I+R	1025	
1122.9	b <sub>1</sub>	I+R	1134	
1213.9	a <sub>1</sub>	I+R	1227	
1252.6	a <sub>1</sub>	I+R	1265	1265
1293.5	a <sub>1</sub>	I+R	1276	
1366.7	a <sub>1</sub>	I+R		1345
1400.8	a <sub>1</sub>	I+R		1377*
1442.1	a <sub>1</sub>	I+R	1433	1433
1454.7	b <sub>1</sub>	I+R	1447	
1456.2	a <sub>1</sub>	I+R		1440
1499.3	b <sub>1</sub>	I+R	1475	
1551.5	a <sub>1</sub>	I+R		1516*
1607.9	b <sub>1</sub>	I+R		1574
1649.2	a <sub>1</sub>	I+R		1620

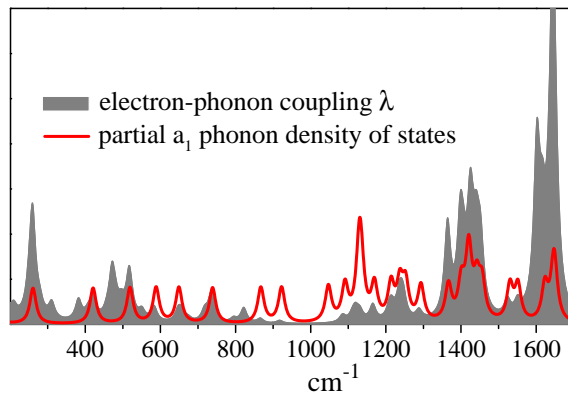


FIG. 4: (Color online) Distribution of the electron-phonon coupling at the  $\Gamma$  point, calculated in the rigid-band approximation in Ref.<sup>12</sup> and partial  $a_1$  phonon density of states. For details of the calculation see<sup>30</sup>.

components in the measured spectrum (see middle panel). In the table, two values corresponding to the same DFT mode indicate the observed splitting.

The precise assignment of the phonon frequencies is particularly important, in connection with the problem of  $ep$  coupling, which in PAHs is usually calculated taking into account only vibronic contributions (see for example Refs.<sup>13,14</sup>). For picene doped with mono-, bi- and tri-anions, as well as with mono-cations, the coupling is non-zero only for modes with  $a_1$  symmetry. According to Ref.<sup>13</sup>, in the case of bi-anion doping, the modes most involved in the  $ep$  coupling are at 253, 724, 1380, 1516  $\text{cm}^{-1}$ . The corresponding values we observe for pure picene are 262, 730, 1377 and 1516  $\text{cm}^{-1}$  (marked by \* in Table 1). A recent calculation by *Casula et al.* for  $\text{K}_3$  picene<sup>11</sup> has shown that this picture is strongly modified by the presence of the potassium, which mediates a strong intermolecular interaction. This result is strongly dependent on the geometrical distribution and concentration of the dopants, and is not representative of *pure* picene.

In Fig. 4 we compare the spectral distribution of the  $ep$  coupling  $\lambda$ , calculated in Ref.<sup>12</sup> using the rigid band approximation, with the partial  $a_1$  phonon density of states to estimate the effect of intermolecular interactions of *pure* crystalline picene<sup>30</sup>. The figure shows that the  $ep$  coupling response is indeed dominated by the  $a_1$  modes, but there are additional contributions clearly coming from modes with different symmetries. Consistently with what we observed in the IR and Raman spectra, the figure shows that intermolecular interactions in *undoped* picene are quite small; this picture could be modified by doping and/or pressure, which could both induce a stronger intermolecular coupling, due to hybridization and/or increased overlap between the molecules.

In conclusion, we have presented high-quality optical data and first-principles calculations for the vibrational spectrum of solid picene. The comparison between experimental and theoretical results enabled us to completely characterize the spectrum, and assign most of the observed vibrational modes. Comparing the theoretical calculations for Raman, IR and electron-phonon spectral function, we have identified picene as solid, with a small intermolecular interaction. The extensive characterization obtained in this study is fundamental for further studies on the effect of pressure and/or doping on bonding and intermolecular interactions in doped polycyclic aromatic hydrocarbons.

## References

- 
- <sup>†</sup> corresponding author: [Paolo.Dore@roma1.infn.it](mailto:Paolo.Dore@roma1.infn.it)
- <sup>1</sup> R. Mitsuhashi, Y. Suzuki, Y. Yamanari, H. Mitamura, T. Kambe, N. Ikeda, H. Okamoto, A. Fujiwara, M. Yamaji, N. Kawasaki, Y. Maniwa, and Y. Kubozono, *Nature* **464**, 76 (2010).
  - <sup>2</sup> X. F. Wang, R. H. Liu, Z. Gui, Y. L. Xie, Y. J. Yan, J. J. Ying, X. G. Luo, and X. H. Chen, *Nature Communications* **2**, 507 (2011).
  - <sup>3</sup> M. Xue, T. Cao, D. Wang, Y. Wu, H. Yang, X. Dong, J. He, F. Li, and G. F. Chen, *Scientific reports* **2**, 389 (2012).
  - <sup>4</sup> H. Mitamura, X. Lee, X. He, Y. Yamanari, Y. Takahashi, Y. Suzuki, Y. Kaji, R. Eguchi, K. Akaike, T. Kambe, et al., *Physical Chemistry Chemical Physics* **13**, 16476 (2011).
  - <sup>5</sup> X. F. Wang, Y. J. Yan, Z. Gui, R. H. Liu, J. J. Ying, X. G. Luo, and X. H. Chen, *Physical Review B* **84**, 214523 (2012).
  - <sup>6</sup> X. F. Wang, X. G. Luo, J. J. Ying, Z. J. Xiang, S. L. Zhang, R. R. Zhang, Y. H. Zhang, Y. J. Yan, A. F. Wang, P. Cheng, G. J. Ye, X. H. Chen, [arXiv:cond-mat/1203.5887](https://arxiv.org/abs/cond-mat/1203.5887) (2012).
  - <sup>7</sup> J. Nagamatsu, N. Nakagawa, T. Muranaka, Y. Zenitani, and J. Akimitsu, *Nature* **410**, 63 (2001).
  - <sup>8</sup> G. Savini, A. C. Ferrari, and F. Giustino, *Physical Review Letters* **105**, 037002 (2010).
  - <sup>9</sup> G. Giovannetti and M. Capone, *Physical Review B* **83**, 134508 (2011).
  - <sup>10</sup> M. Kim, B. I. Min, G. Lee, H. J. Kwon, Y. M. Rhee, and J. H. Shim, *Physical Review B* **83**, 214510 (2011).
  - <sup>11</sup> M. Casula, M. Calandra, G. Profeta, and F. Mauri, *Physical Review Letters* **107**, 137006 (2011).
  - <sup>12</sup> A. Subedi and L. Boeri, *Physical Review B* **84**, 020508 (2011).
  - <sup>13</sup> T. Kato, T. Kambe, and Y. Kubozono, *Physical Review Letters* **107**, 077001 (2011).
  - <sup>14</sup> T. Sato, N. Iwahara, and K. Tanaka, *Physical Review B* **85**, 161102 (2012).
  - <sup>15</sup> A. De, R. Ghosh, S. Roychowdhury, and P. Roychowdhury, *Acta Crystallographica Section C* **41**, 907 (1985).
  - <sup>16</sup> A. Girlando, M. Masino, I. Bilotti, A. Brillante, R.G. Della Valle, and E. Venuti, *Physical Chemistry Chemical Physics*, **14**, 1694 (2012).
  - <sup>17</sup> D. Di Castro, E. Cappelluti, M. Lavagnini, A. Sacchetti, A. Palenzona, M. Putti, and P. Postorino, *Physical Review B* **74**, 100505 (2006).
  - <sup>18</sup> C. Marini, C. Mirri, G. Profeta, S. Lupi, D. Di Castro, R. Sopracase, P. Postorino, P. Calvani, A. Perucchi, S. Massidda, G.M. Tropeano, M. Putti, A. Martinelli, A. Palenzona, and P. Dore, *Europhysics Letters* **84**, 67013 (2008).
  - <sup>19</sup> S. Baroni, S. de Gironcoli, A. Dal Corso, and P. Giannozzi, *Reviews of Modern Physics* **73**, 515 (2001).
  - <sup>20</sup> X. Blase, C. Attaccalite, and V. Olevano, *Physical Review B* **83**, 115103 (2011).
  - <sup>21</sup> H. Okamoto, N. Kawasaki, Y. Kaji, Y. Kubozono, A. Fujiwara, and M. Yamaji, *Journal of American Chemical Society* **130**, 10470 (2008).
  - <sup>22</sup> L. Malavasi 2011 (private communication)
  - <sup>23</sup> S. Lupi, A. Nucara, A. Perucchi, P. Calvani, M. Ortolani, L. Quaroni, and M. Kiskinova, *Journal of the Optical Society of America B* **24**, 959 (2007).
  - <sup>24</sup> M. Lazzeri and F. Mauri, *Physical Review Letters* **90**, 036401 (2003).
  - <sup>25</sup> All calculations are performed using the QUANTUM ESPRESSO code: P. Giannozzi et al., *Journal of Physics: Condensed Matter* **21**, 395502 (2009).
  - <sup>26</sup> We used the pseudopotentials C.pz-vbc.UPF and H.pz-vbc.UPF from <http://www.quantum-espresso.org>.
  - <sup>27</sup> <http://www.webqc.org/printable-symmetrypointgroup-ct-c2v.html>



- <sup>28</sup> D. L. Rousseau, R. P. Bauman, and S. P. S. Porto, *Journal of Raman Spectroscopy* **10**, 253 (1981).
- <sup>29</sup> Note that Girlando et al. choose a different orientation of the coordinate system for the molecule, and therefore their definition of  $b_1$  and  $b_2$  modes is interchanged.
- <sup>30</sup> The data shown as grey shaded region in fig. 4 are the  $\lambda_{\mathbf{q},\nu}$  data at the  $\Gamma$  point, for a doping of  $x = 3$  electrons/molecule in the rigid band approximation. In order to have a well-converged spectral distribution, we divided the  $\lambda_{\mathbf{q},\nu}$  calculated in Ref.<sup>12</sup>, by the corresponding nesting function ( $\chi(\mathbf{q})$ ) (see also Ref.<sup>11</sup> for details).

### Supplementary information

DFT Frequency	Mode Symmetry.	Mode activity	IR Intensity	Raman Intensity
203.8	b <sub>2</sub>	I+R	4.19	0.09
237.8	b <sub>2</sub>	I+R	6.39	0.02
260.8	a <sub>1</sub>	I+R	0.02	6.11
283.6	b <sub>1</sub>	I+R	0.00	0.08
309.0	a <sub>2</sub>	R	0.00	0.29
395.8	a <sub>2</sub>	R	0.00	1.39
419.5	b <sub>2</sub>	I+R	14.30	0.01
420.8	a <sub>1</sub>	I+R	0.10	0.06
467.6	a <sub>2</sub>	R	0.00	0.06
473.6	b <sub>1</sub>	I+R	0.16	0.47
481.2	b <sub>1</sub>	I+R	3.02	0.00
501.4	b <sub>2</sub>	I+R	0.06	0.06
519.0	a <sub>1</sub>	I+R	0.00	0.43
520.1	b <sub>1</sub>	I+R	2.52	0.03
523.3	b <sub>2</sub>	I+R	13.80	0.02
555.3	a <sub>2</sub>	R	0.00	0.01
555.8	b <sub>1</sub>	I+R	0.86	0.25
588.5	a <sub>1</sub>	I+R	0.13	2.15
591.1	a <sub>2</sub>	R	0.00	0.15
649.2	a <sub>1</sub>	I+R	0.03	2.61
660.7	b <sub>2</sub>	I+R	0.05	0.19
679.8	b <sub>1</sub>	I+R	3.77	0.08
710.8	a <sub>2</sub>	R	0.00	0.22
713.4	b <sub>2</sub>	I+R	59.7	1.65
729.8	a <sub>2</sub>	R	0.00	3.79
738.9	a <sub>1</sub>	I+R	0.04	9.44
742.5	b <sub>2</sub>	I+R	87.0	0.00
781.2	a <sub>2</sub>	R	0.00	0.59
787.0	b <sub>2</sub>	I+R	100.00	0.00
791.8	b <sub>1</sub>	I+R	0.37	0.00
816.0	b <sub>2</sub>	I+R	0.83	2.07
846.9	a <sub>2</sub>	R	0.00	1.02
864.1	b <sub>2</sub>	I+R	1.45	0.00
867.3	a <sub>1</sub>	I+R	0.26	1.39
870.2	b <sub>2</sub>	I+R	9.46	0.67
870.6	a <sub>2</sub>	R	0.00	0.24
881.0	b <sub>1</sub>	I+R	0.00	0.47
922.5	a <sub>1</sub>	I+R	0.00	1.60
930.2	a <sub>2</sub>	R	0.00	3.65
932.1	b <sub>2</sub>	I+R	3.94	0.34
942.4	a <sub>2</sub>	R	0.00	0.00

DFT Frequency	Mode Symmetry.	Mode Activity	IR Intensity	Raman Intensity
947.7	a <sub>2</sub>	R	0.00	1.50
952.8	b <sub>2</sub>	I+R	1.19	0.06
966.2	b <sub>2</sub>	I+R	0.16	0.04
966.5	a <sub>2</sub>	R	0.00	0.03
1047.1	a <sub>1</sub>	I+R	0.27	11.10
1048.8	b <sub>1</sub>	I+R	0.21	0.07
1050.1	b <sub>1</sub>	I+R	4.29	0.27
1091.3	a <sub>1</sub>	I+R	0.76	0.13
1122.9	b <sub>1</sub>	I+R	1.72	0.32
1129.4	a <sub>1</sub>	I+R	0.34	0.80
1130.7	b <sub>1</sub>	I+R	0.06	1.24
1134.7	a <sub>1</sub>	I+R	0.00	0.21
1148.8	b <sub>1</sub>	I+R	0.00	0.84
1169.5	a <sub>1</sub>	I+R	0.77	4.19
1213.9	a <sub>1</sub>	I+R	11.80	2.29
1216.0	b <sub>1</sub>	I+R	3.12	0.09
1237.3	a <sub>1</sub>	I+R	0.07	5.41
1240.3	b <sub>1</sub>	I+R	0.13	1.00
1247.6	b <sub>1</sub>	I+R	0.31	0.01
1252.6	a <sub>1</sub>	I+R	3.69	3.75
1293.5	a <sub>1</sub>	I+R	4.84	2.44
1337.3	b <sub>1</sub>	I+R	0.28	0.12
1366.7	a <sub>1</sub>	I+R	0.38	17.90
1400.8	a <sub>1</sub>	I+R	1.65	85.00
1405.3	b <sub>1</sub>	I+R	0.45	0.31
1420.7	a <sub>1</sub>	I+R	0.07	6.43
1427.8	b <sub>1</sub>	I+R	0.05	0.28
1433.7	b <sub>1</sub>	I+R	0.13	6.09
1442.1	a <sub>1</sub>	I+R	4.74	76.50
1454.7	b <sub>1</sub>	I+R	7.69	0.76
1456.2	a <sub>1</sub>	I+R	0.08	100.00
1499.3	b <sub>1</sub>	I+R	6.80	0.07
1530.4	a <sub>1</sub>	I+R	0.51	1.09
1551.5	a <sub>1</sub>	I+R	0.05	13.10
1558.9	b <sub>1</sub>	I+R	1.23	0.47
1607.9	b <sub>1</sub>	I+R	0.02	10.40
1623.3	a <sub>1</sub>	I+R	3.56	0.68
1635.7	b <sub>1</sub>	I+R	0.89	4.52
1646.2	a <sub>1</sub>	I+R	0.75	7.30
1649.2	a <sub>1</sub>	I+R	0.63	21.20
1655.5	b <sub>1</sub>	I+R	0.02	2.08

DFT phonon modes in the frequency range 200-1700 cm<sup>-1</sup>. For each mode, calculated DFT frequency, symmetry, optical activity, and intensity of the IR and/or Raman frequency are reported. Intensities are normalized to a maximum value of 100.00.

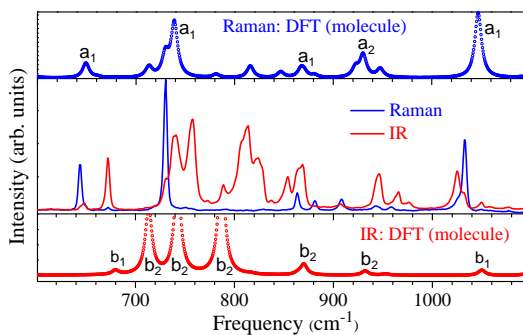


FIG. 5: Comparison between the measured IR and Raman spectra (middle panel), DFT Raman (upper panel), and IR (lower panel) spectra in the range  $600 - 1100 \text{ cm}^{-1}$ . The computed DFT stick spectra are convoluted with a Lorentzian profile with  $10 \text{ cm}^{-1}$  linewidth to ease comparison with experiment.

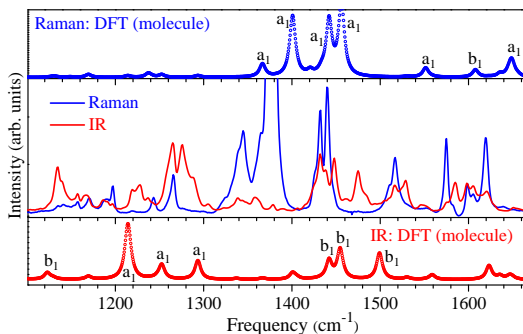


FIG. 6: Comparison between the measured IR and Raman spectra (middle panel), DFT Raman (upper panel), and IR (lower panel) spectra in the range  $1100 - 1700 \text{ cm}^{-1}$ . The computed DFT stick spectra are convoluted with a Lorentzian profile with  $10 \text{ cm}^{-1}$  linewidth to ease comparison with experiment.

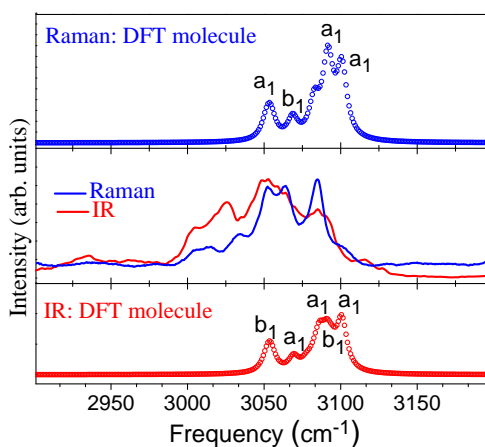


FIG. 7: Comparison between the measured IR and Raman spectra (middle panel), DFT Raman (upper panel), and IR (lower panel) spectra in the frequency range of the C-H stretching ( $3000 - 3250 \text{ cm}^{-1}$ ) which is not of direct interest in the present paper. Notice that the measured Raman and IR spectra have been normalized to the same maximum. Like in other frequency ranges, the computed DFT stick spectra are convoluted with a Lorentzian profile with  $10 \text{ cm}^{-1}$  linewidth to ease comparison with experiment.